Lecture Notes in Networks and Systems 153

Nenad Mitrovic
Goran Mladenovic
Aleksandra Mitrovic *Editors*

Experimental and Computational Investigations in Engineering

Proceedings of the International Conference of Experimental and Numerical Investigations and New Technologies, CNNTech 2020

Springer

Lecture Notes in Networks and Systems

Volume 153

The series "Lecture Notes in Networks and Systems" publishes the latest developments in Networks and Systems—quickly, informally and with high quality. Original research reported in proceedings and post-proceedings represents the core of LNNS.

Volumes published in LNNS embrace all aspects and subfields of, as well as new challenges in, Networks and Systems.

The series contains proceedings and edited volumes in systems and networks, spanning the areas of Cyber-Physical Systems, Autonomous Systems, Sensor Networks, Control Systems, Energy Systems, Automotive Systems, Biological Systems, Vehicular Networking and Connected Vehicles, Aerospace Systems, Automation, Manufacturing, Smart Grids, Nonlinear Systems, Power Systems, Robotics, Social Systems, Economic Systems and other. Of particular value to both the contributors and the readership are the short publication timeframe and the world-wide distribution and exposure which enable both a wide and rapid dissemination of research output.

The series covers the theory, applications, and perspectives on the state of the art and future developments relevant to systems and networks, decision making, control, complex processes and related areas, as embedded in the fields of interdisciplinary and applied sciences, engineering, computer science, physics, economics, social, and life sciences, as well as the paradigms and methodologies behind them.

**** Indexing: The books of this series are submitted to ISI Proceedings, SCOPUS, Google Scholar and Springerlink ****

More information about this series at http://www.springer.com/series/15179

Nenad Mitrovic · Goran Mladenovic ·
Aleksandra Mitrovic
Editors

Experimental and Computational Investigations in Engineering

Proceedings of the International Conference of Experimental and Numerical Investigations and New Technologies, CNNTech 2020

Springer

Editors
Nenad Mitrovic
Faculty of Mechanical Engineering,
Department for Process Engineering
and Environmental Protection
University of Belgrade
Belgrade, Serbia

Goran Mladenovic
Faculty of Mechanical Engineering,
Department for Production Engineering
University of Belgrade
Belgrade, Serbia

Aleksandra Mitrovic
Faculty of Information Technology
and Engineering
University Union - Nikola Tesla
Belgrade, Serbia

ISSN 2367-3370 ISSN 2367-3389 (electronic)
Lecture Notes in Networks and Systems
ISBN 978-3-030-58361-3 ISBN 978-3-030-58362-0 (eBook)
https://doi.org/10.1007/978-3-030-58362-0

This Springer imprint is published by the registered company Springer Nature Switzerland AG
The registered company address is: Gewerbestrasse 11, 6330 Cham, Switzerland

Experimental and Numerical Analysis of Stress-Strain Field of the Modelled Boiler Element

Milena Rajić[1(✉)], Dragoljub Živković[1], Milan Banić[1], Marko Mančić[1], Miloš Milošević[2], Taško Maneski[3], and Nenad Mitrović[3]

[1] Faculty of Mechanical Engineering, University of Nis, Nis, Serbia
milena.rajic@masfak.ni.ac.rs
[2] Innovation Center of Faculty of Mechanical Engineering, University of Belgrade, Belgrade, Serbia
[3] Faculty of Mechanical Engineering, University of Belgrade, Belgrade, Serbia

Abstract. Hot water boilers are most commonly used devices in thermal and industrial plants for heat production. Boilers elements are exposed to high pressures and temperatures during boiler operation. Non-stationary working regimes of boiler may lead to breakdowns and fatigue of boiler elements. There are numerous cases of breakdowns of such units, which lead to reduced reliability and safety of the plant. In order to avoid this state, certain investigation should be made that would examine the influence of different regimes on the boiler structure. Lack of available data concerning the temperature as well as stress-strain field in boiler elements led us to perform such kind of experiment. This paper presents results of numerical analysis performed on the modelled boiler. Validation of the numerical model was performed based on experimental results obtained using DIC (Digital Image Correlation) method by using Aramis system. The character of parameters change, such as strain and stress, occurring in the critical zones of boiler elements can be verified both by experimental and numerical results. In this paper the novel approach of experimental and numerical analysis is presented. The method can be used and conducted in similar units for testing on different loads or working regimes, as well as to improve the safety and reliability of similar pressure vessel units.

Keywords: Hot water boiler · Finite element method · Digital Image Correlation

1 Introduction

Hot water boilers, especially boilers with fire tube where the combustion takes place, are widely used in process industry. Exploitation experience indicates constant and permanent breakdowns occurring as a result of accidental states of individual boiler elements. Studies done before in this field indicate certain critical boiler elements that may have influence on the reliability and safety of the entire unit [1–6].

N. Mitrovic et al. (Eds.): CNNTech 2020, LNNS 153, pp. 257–273, 2021.
https://doi.org/10.1007/978-3-030-58362-0_15

One of the most critical elements is certainly the tube plate, located on the first and second flue reversing chamber. Design calculations of boiler elements are done by using existing norms and standards that impose certain safety factors for stress calculations that is allowed in nominal regime [7–13]. Very often a large value of safety factor can lead to over-dimensions of elements thickness, which not only can increase design costs but also to have an unfavourable impact to the strength of the structure. The paradox in this case is that, when the wall of the tube plate is wider, the lower are the stresses caused by pressure, but the thermal stresses are higher under the same parameters. Then, the wall thickness should be chosen to minimize the total cumulative load - pressure load and thermal load [14]. It should not be allowed to have any non-elastic deformation in these barring element constructions.

Exact application of analytical elasticity method is not possible due to the complex structure of the boiler elements. For boiler structure calculation, Finite Element Method FEM is already used in numerous studies [7–12, 14–21]. FEM represents a numerical method that enables modeling and calculation of complex constructions and problems by dividing the structure into a numerous finite elements with correct geometric form, whose behaviour is possible to describe.

Published studies done in this field, with this specific unit, indicate the lack of available data on measurements conducted on boiler itself or boiler elements. Stress-Strain analysis of hot water boiler done by FEM [7–12, 14–21] are based on data given in standards or in manufacturer documentation, but present general averaged data. There is no evidence of experimental data that can be used to determine the construction temperature field of the boiler's element, neither stress-strain field measured in any part in this type of boiler. One of the limitations of experimental procedure is high cost of experiment that should be performed. Boilers are high expensive pressure vessel unit, and therefore experiments are limited to certain part of the boiler that can be easily repaired and not endangered the essential part of the unit. Not neglecting that, this type of boilers operate in high temperature and pressure regime, therefore security and safety level of the plant and also the personnel involved in experimental procedure is also one of the limitations. One of the reasons for not having this kind of experiments is the limitation of experimental equipment and quality data that would be collected. Conventional methods of measuring temperature (or stress/strains) filed of boiler construction would give us the data in singular points. The distribution of stress field would be also averaged.

Having in mind all the presented limitations, the new approach of an experimental method has been introduced. The suitable model of boiler construction was made, maintaining the rigidity of the elements in the real boiler unit (that are exposed to the real operating loads) and the model (with the maximum allowed loads that can be simulated in the laboratory conditions). The presented method included the laboratory testing where several measurement procedures can be conducted in different loads, measurement conditions etc. The performed measurement includes: temperature measurement of critical part of the model by using thermocouple, strain measurement of the same critical part by strain gauge, the 3D Digital Image Correlation (DIC) method for stress-strain measurement. The numerical calculation of the model with all real time parameters data was performed and presented. Considering a large amount of data that is obtained in

this experimental procedure, only the critical parts of the tube plate (as one of the most critical part of this type of boilers) in critical regimes are presented.

The construction model testing or its structure is of high importance especially in cases of prototype testing in solving the constructions design problems. Using the method of experimental analysis, a number of relevant data are usually obtained for assessing the load capacity and stability of the structure. Particularly important are the data related to the effect of local stress concentrations, determining the area of plastic deformation, the fracture mechanism, as well as the impact of mechanical characteristics changes depending on time and temperature. Experimental methods are of the highest importance, especially in those cases where due to the complexity of the problem the theoretical model is almost impossible or very difficult to solve. Experimental methods are particularly important in cases where the significant stress concentrations on the construction occur, which in operating conditions very often lead to the failures and breakdowns.

The 3D Digital Image Correlation (DIC) method represents the novel method of stress-strain measurement [22–34]. It enables full-field stress-strain measurements. During one measurement procedure big datasets are obtained that in conventional experimental method would replace a large number of strain gauges and therefore significantly reduces experimental planning time and preparation and also costs. Also numerical methods such as finite element method enables results of full covered stress-strain field, that can be easily verified by the data obtained from experiment. The main idea in this study was to link the numerical experiment of the model within finite element method to experimental measurement and to have not only the data that is verified by using different measurement methods, but also the interconnection between the numerical and real model testing that can be used also for similar units with the same load nature.

This paper analyzes critical elements of the hot water boiler by experimental data obtained from its model and improved numerical model in order to analyze constrains and loads the model is exposed to and to have fully-covered stress-strain field obtained from experimental data.

2 Design Parameters and Geometrical Data

In order to perform the experimental laboratory study, the suitable model for testing was design. As it is mentioned before, real boiler unit is huge, and as such it is not able to fit the laboratory. It was necessary to scale the object to the appropriate dimensions of the model, which could easily be installed in laboratory. The aim of the model forming (design) was to preserve the rigidity of the model and the real object, since stress-strain analysis of tube plate would be examined under different conditions. All dimensions were scaled 10 times, including the thickness of the tube plates. The model includes the plain tube as the fire tube, instead of the Fox corrugated flame tube, with the appropriate thickness so that the rigidity of that element would be identical in the conditions of the real object. Due to complexity of the layout and the number of flue pipes of the real object, in which there are 208 flue pipes, another approximation was made. Namely, flue pipes scaled 10 times, would give an extremely dense pipe network in the model, which is impossible to provide on the market because of its dimensions. This is the

reason where 45 "full tubes" or rods, distributed on the tube plate of the model, were adopted, following the schedule and distribution of the flue pipes on the real object. The dimensions of these rods will not affect the rigidity of the structures, which means that it would remain identical or substantially the same in the already defined critical points of the model and the real object. Geometric model is presented in Fig. 1.

3 Numerical Analysis of the Model

The geometric model was transformed into the discretized FE model with the application of advanced meshing tool capable of creating adaptive discrete model. The discretized model consisted of 438128 nodes, which formed 352921 finite elements. The discretized model of the analyzed boiler is presented in Fig. 2. The finite element mesh has an identical topology for thermal and structural analysis, but these meshes are formed by different types of finite elements. The resulting meshes are automatically unified into a unique hybrid finite element mesh in which the definite topology overlaps the finite elements relevant to individual analyzes. In the analysis, the materials that are used (which correspond to the real boiler construction) have the characteristics [35, 36]. Working loads were also defined, which were simulated in laboratory conditions. By analyzing the structural load of the design model, the loads can be determined as:

1. loads resulting from the weight of the model's elements;
2. loads resulting from the thermal expansion on higher temperatures;
3. real boiler operating loads that should have been simulated.

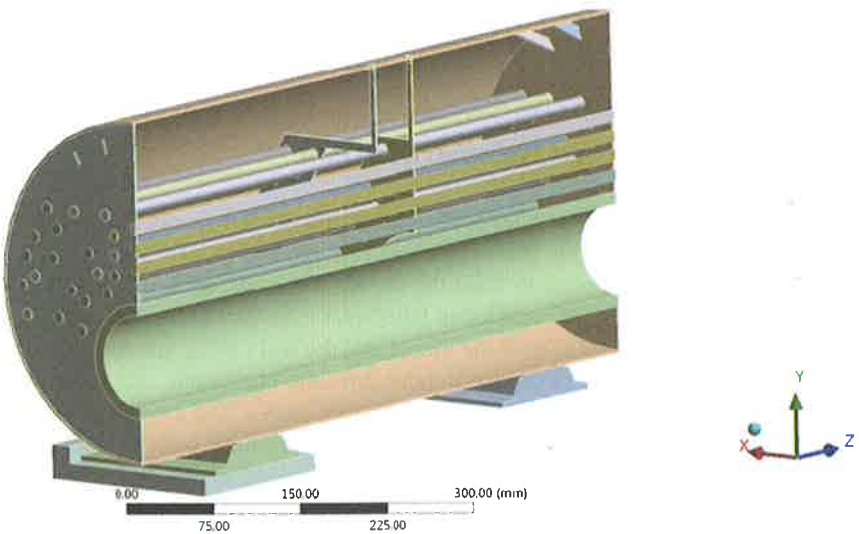

Fig. 1. Symmetrical geometric model

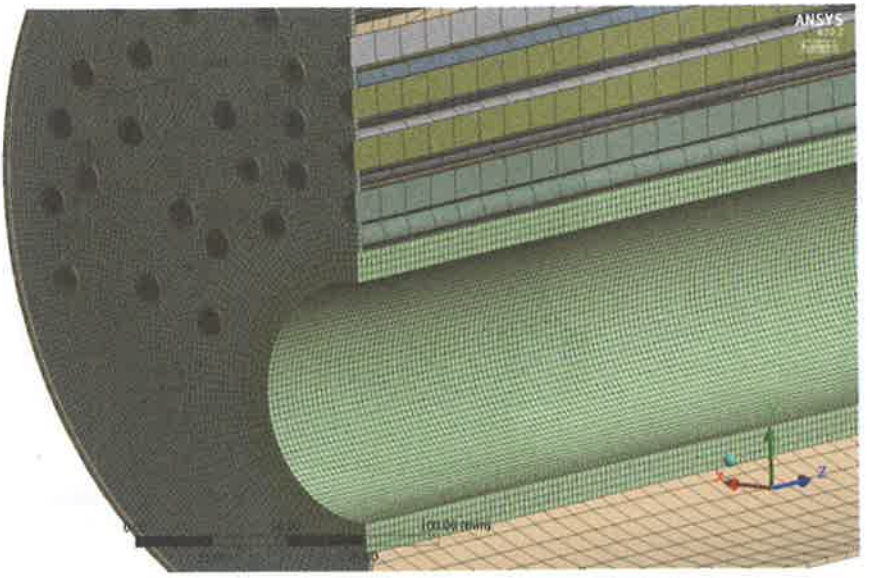

Fig. 2. Numerical model of discretized structure of the model

Beside the thermal and hydraulic pressure loads, other mechanical loads were also accounted during the static structural analysis: the gravity force and the hydrostatic water pressure.

Below (Fig. 3 and 4) the equivalent (Von Misses) stresses of the tube plate element are presented. In Fig. 3 the model was exposed to 5 bar pressure on the water side and without any source of heating (cold phase) and in Fig. 4 the model was under 5 bar pressure on the water side and with thermal load that was simulated with heaters inside the fire tube. The results of analysis show that the maximal stresses occur on the upper part of the tube plate in the case without heating (Fig. 3) and on the part of the tube plate closer to the fire tube outlet (Fig. 4). These are the critical locations, where the particular attention was made. Therefore, on these locations was the main focus in presenting the following experimental results. It should be noted that the boiler, as real object, shows specific sensibility in exactly those specific locations. As is was previously mentioned, one of the critical elements of the boilers is the tube plate and especially the part that is near the fire tube outlet, where combustion takes place and where the maximum temperatures are and where accidents often occur. The major breakdowns of the hot water fire-tube boilers are caused by the damage and failures of the welding joints in these elements [37, 38].

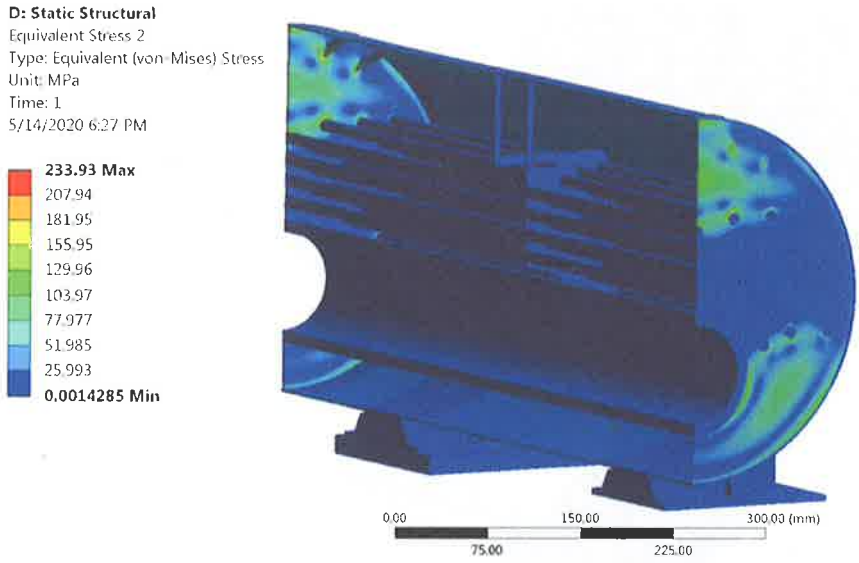

Fig. 3. Equivalent (von-Mises) stresses of the model exposed to 5 bar pressure on the water side-cold state

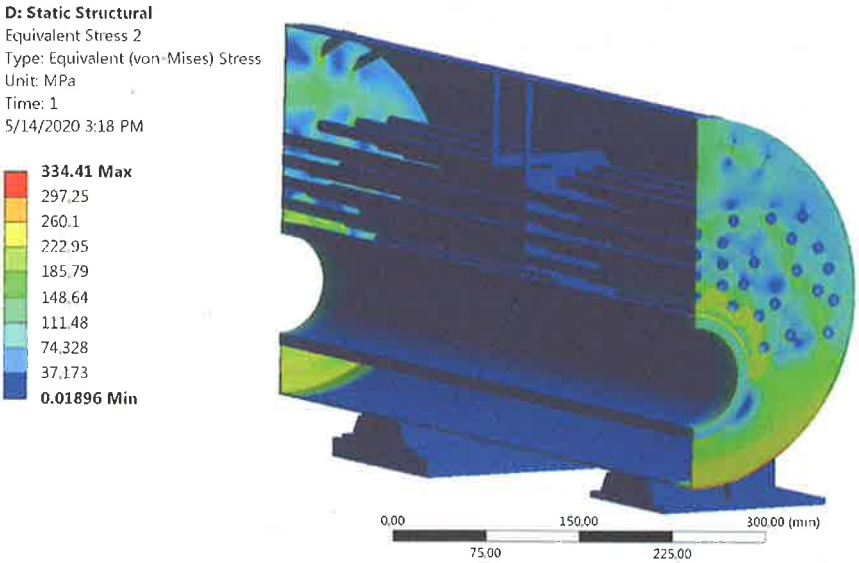

Fig. 4. Equivalent (von-Mises) stresses of the model exposed to 5 bar pressure on the water and with heaters inside the fire tube

4 Experimental Procedure

The aim of experimental testing was to verify the numerical calculation of the model with physically installed model in the laboratory. In this manner, reliability and accuracy of the numerical calculation of the defined model with the given loads would be presented. The similarity of the appearance and character of the change in physical variables (stress-strain) is expected by comparing the results of the experiment on the model and the real object.

The experimental methods used are strain gauge method and methods for contactless measurement of stress and deformation (DIC). The given load is symmetric, so that it allows (along with the already existing symmetry of the construction itself) parallel measurement of the strain gauge and the Digital Image Correlation (DIC) system. Two strain gauges are placed at the selected points on the same half of the structure (i.e. the tube plate), and on the other half they will be used to record correspondence fields with cameras (Fig. 5).

Fig. 5. The strain gauges locations and measuring areas for DIC system

For DIC system for strain measurement, appropriate procedures are defined by producer and developed for experimental testing. The experiment was performed according to following procedure: sample preparation (the measuring surface must have a pattern with contrast to clearly allocate the pixels in camera images), measuring volume selection (selecting the measuring volume is based on the sample size), system calibration (for certain measuring volume, the appropriate calibration panel is used for sensor configuration), sample positioning (the boiler model was positioned in a way that appropriate tube plate was fully exposed to cameras, the one side of the boiler was fixed as it is in real operating conditions), measurement (after calibration, measurement procedure was performed. The pressure on the water side was gradually loaded, up to 5 bars. Digital

images were recorded 60 s after the loading), data processing (recorded data is in a form of report, that can be further analyze).

Experiment was performed both in a cold state, i.e. without the installation of heaters and in the warm state, i.e. with the installed heaters. The recordings of each measuring area (6 marked measuring area) were performed in phases, with different loads - pressures on the water side (the boiler was previously filled with water). Filling the boiler with water and setting the pressure was carried out by a manual pump. The pump is connected to the model with the valve to allow constant pressure during the test. The measuring pressure was in interval 1–5 bar with 60 s stabilization time period between the measured pressure set. To perform the experiment as faithfully as possible in laboratory conditions, the idea was to install a heater, inside the fire tube, whose power will be able to be controlled and adjusted during the experiment. For testing purposes, a heater with a power of 5 kW was made, which consists of 6 individual heaters. It was possible to activate the heaters individually, all at once or in the desired combination, in order to achieve equal heating of the structure. The heater also had a potentiometer, which allowed regulating the power of the heaters and maintaining a constant power over time.

5 Results and Discussion

In the experimental procedure, the critical measuring areas were identified, where the stress strain field has its maximum. The first phase of the examination procedure, the installation without heaters, in the cold state, gave us the significant results.

Von Mises strain results are presented for the first measuring area, Fig. 6. The examined condition was under max test pressure of 5 bar. Experimental data is presented graphically as function of section length. Scale in % is given on ordinate of Fig. 6. The 3D Von Mises strain field across the sample surface (the first measuring area) (Fig. 6c and d) is presenting the highest measured strains (orange color). Von Mises strain values are also given as section length function (Fig. 6a and b). Strain stages (0–3) represent pressure increase, where stage 0 represents beginning of the experiment to stage 3 where maximal test pressure is for the experiment.

In (Fig. 6d) it is shown a line which "imitates" virtual strain gauge. The Aramis system software provides ability to determine the distance between any two points in any moment of experiment. The horizontal line here is in the same place as the real strain gauge in order to verify results and compare.

In Table 1, the comparison of obtained results by using strain gauge, the Aramis system and results obtained numerically in Ansys software. The results of certain pressures values are missing form DIC Aramis system because the measurement was conducted in stages of (2 bar, 3.5 bar, 5 bar), also measured results from strain gauge under pressure of 3.5 bar also missing, while the results are only taken for pressure of 4 and 5 bar. The results form experimental and numerical analysis are presented more detailed in [39].

The results from strain gauge and obtained numerically have significantly match. Therefore, the numerical model can be verified under different pressure loads by the results obtained from the measurements of strain gauge. The 3D DIC Aramis system has certain limitation, especially when there are small displacements. There are deviations about 30% in experimental results compared to numerical model or measured strain by

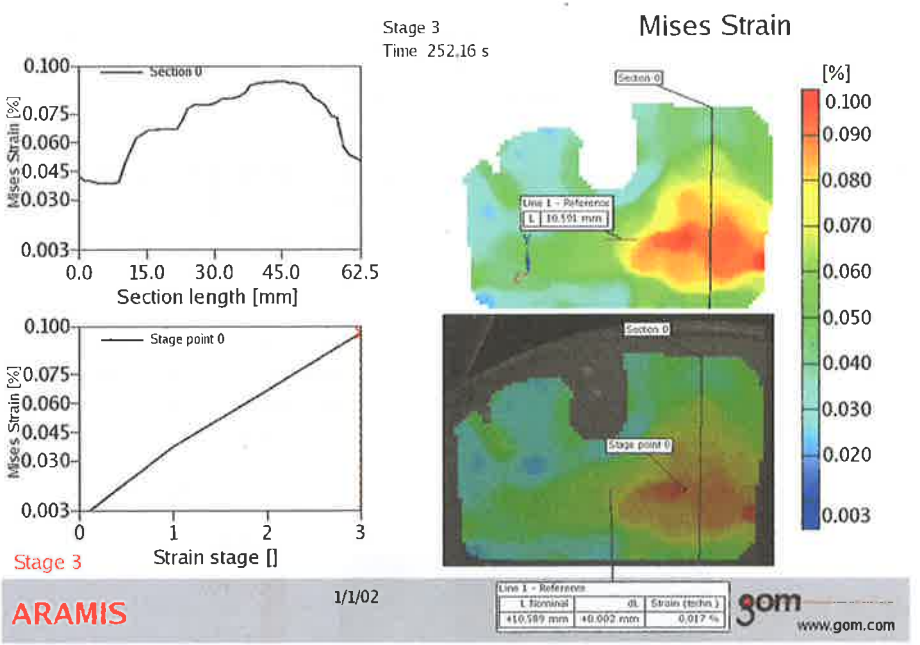

Fig. 6. Experimental results of Von Mises strain for maximal test pressure of 5 bar. a) Von Mises strain as a function of distance for marked Section. b) Von Mises strain as a function of strain stage. c) Von Mises strain field. d) Sample image with overlaying Von Mises strain field (measuring area 1).

Table 1. Resulting strain value measured by strain gauge, DIC Aramis system, results of FEM

Pressure [bar]	Strain gauge	Aramis system	FEM Ansys
1	$3.2931 \cdot 10^{-5}$	/	$3.0189 \cdot 10^{-5}$
2	$5.7071 \cdot 10^{-5}$	$9.44376 \cdot 10^{-5}$	$6.01 \cdot 10^{-5}$
3	$8.5409 \cdot 10^{-5}$	/	$8.9972 \cdot 10^{-5}$
3.5	/	$1.30344 \cdot 10^{-4}$	$1.009 \cdot 10^{-4}$
4	$1.47662 \cdot 10^{-4}$	/	$1.201 \cdot 10^{-4}$

strain gauge. The advantage of this measurement method is the whole measured strain area.

The second phase of experimental procedure includes the thermal strains, simulated with suitable adjustable heaters installed inside the fire tube. The properties of the heaters allow us to set the desired amount of heat that we want to keep during the examination phase. In order to simulate the real boiler conditions in described experiment, the heaters were design to be installed inside the fire tube. The heat transfer mechanisms were similar as the ones in the real hot water boiler. On the other hand, the constant water pressure was maintained by a pump. The measurements were perform on the desired pressure of

the water inside the model and controlled temperature of the plate wall. The comparable results are presented in the Table 2 but only for the results obtained with Aramis system and with FEM analysis in Ansys software package.

Table 2. Resulting strain measured by DIC Aramis system and FEM analysis with heating

Pressure [bar]	Aramis system	FEM Ansys
0.5	$9.5840 \cdot 10^{-5}$	$2.3769 \cdot 10^{-5}$
1.5	$1.9168 \cdot 10^{-4}$	$7.624 \cdot 10^{-5}$
2.5	$2.8752 \cdot 10^{-4}$	$1.3688 \cdot 10^{-4}$
3.5	$4.7920 \cdot 10^{-4}$	$2.1151 \cdot 10^{-4}$
5	$8.6256 \cdot 10^{-4}$	$2.9284 \cdot 10^{-4}$

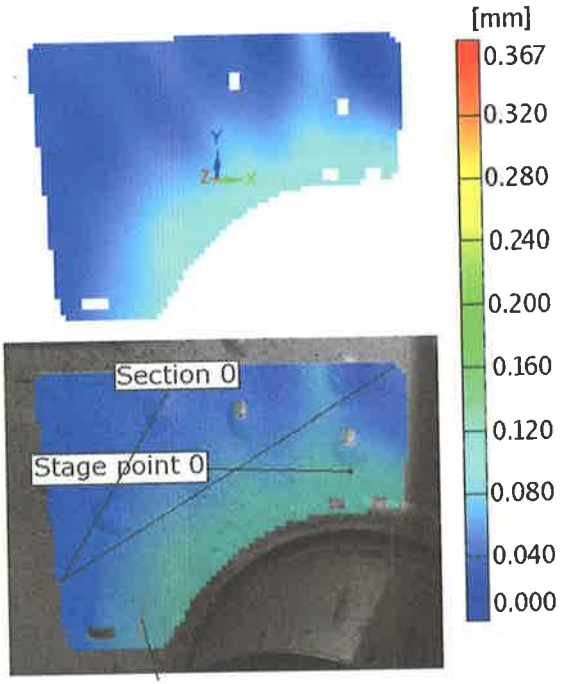

Fig. 7. Results of directional deformation measured by DIC Aramis system - pressure load 1.5 bar

Results obtained by Aramis system and the FEM in Ansys software show significant matches in different loads with a similar temperature field. As already noted, Aramis system has certain limitation, especially in cases of small displacements/deformations, as is the presented case (Table 2).

The results of directional deformation are presented from Aramis system and numerical model done in Ansys software, as it can be seen on Fig. 7 and Fig. 8. The pressure

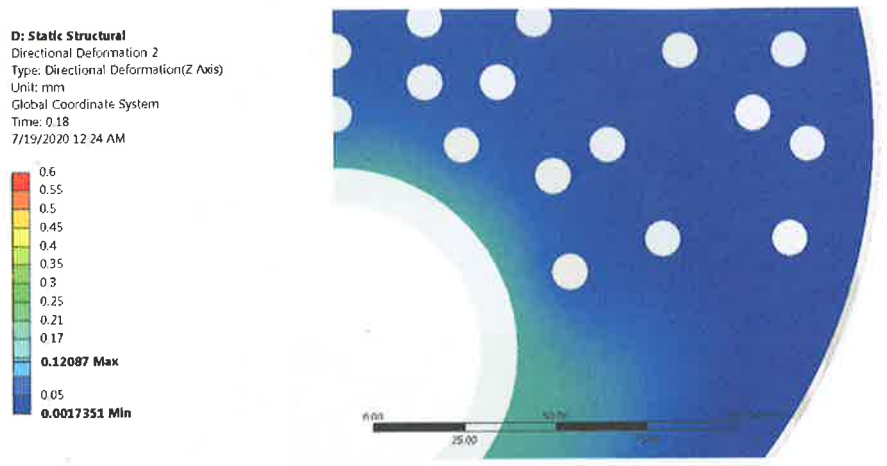

Fig. 8. Results of directional deformation done numerically by Ansys software package - pressure load 1.5 bar

load was 1.5 bar on the water side and the temperature of the inner surface of the fire tube was maintained approx. 90 °C. The distribution of deformation field is quite the same as well as the critical zones.

Results of measured directional deformation by Aramis system and results obtained numerically by finite element method are mostly the same. The critical zones are identified as well as the measured deformations (in critical zone 0.04–0.12 mm). More precisely, the minimal directional deformation under the test pressure of 1.5 bar obtained in Ansys is $1.7351 \cdot 10^{-3}$ mm and maximal is 0.12087 mm.

The next presented experimental stage, was under pressure load of 3.5 bar. The result of directional deformation done by Aramis and numerical method by Ansys is presented in Fig. 9 and 10.

The obtained results from the measured directional deformation by Aramis system and results obtained numerically by finite element method have significant matches. The critical zones are identified as well as the measured deformations (in critical zone 0.15–0.3 mm). The results obtained in Ansys are: the minimal directional deformation under the test pressure of 3.5 bar is $3.3521 \cdot 10^{-3}$ mm and maximal is 0.24365 mm.

In order to analyze one more stage in the conditions with heated surfaces, one more case is presented with the maximal pressure load of 5 bar and it represents the last stage in analysis. These results are presented in Fig. 11 and 12, i.e. the result of directional deformation done by Aramis and numerical method by Ansys, respectively.

The critical zone is now wider in both cases (in critical zones 0.40–0.50 mm). The distribution of directional deformation field has similar position. Minimal deformation in this stage is $7.6147 \cdot 10^{-3}$ mm and maximal 0.51549 mm.

These results are presented in Table 3 as well. It can be seen that in three analyzed cases, there are significant matches with both experimental and numerical results. The deformation field of analyzed plate is quite similar. Having that in mind, the critical parts as well as the critical elements are identified both in numerical and experimental analysis. The experimental procedure on the model had the aim to confirm the phenomenon of

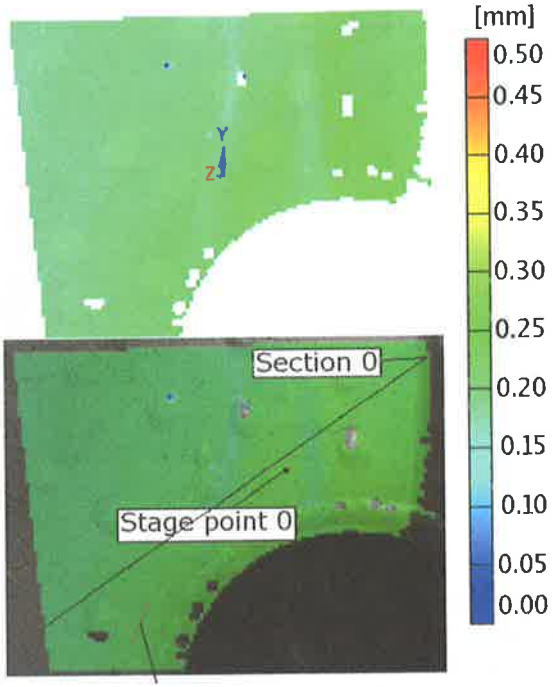

Fig. 9. Results of directional deformation measured by DIC Aramis system - pressure load 3.5 bar

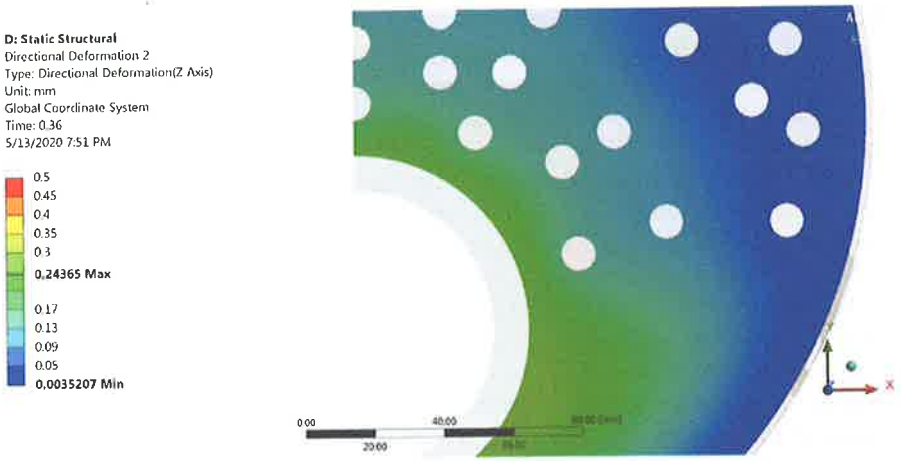

Fig. 10. Results of directional deformation done numerically by Ansys software package - pressure load 3.5 bar

formation and characteristics of deformations of the modeled construction with deformations that occur on a real object. The main goal was to examine the occurrence and characteristics of stresses due to bending of the most sensitive part - the pipe plate of

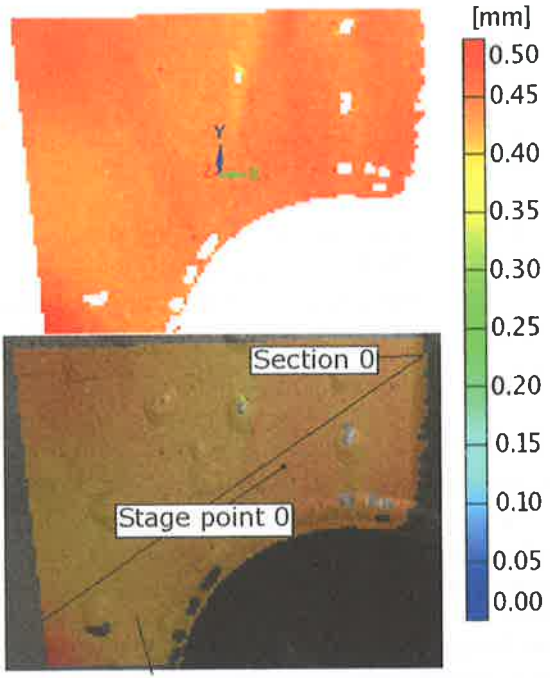

Fig. 11. Results of directional deformation measured by DIC Aramis system - pressure load 5 bar

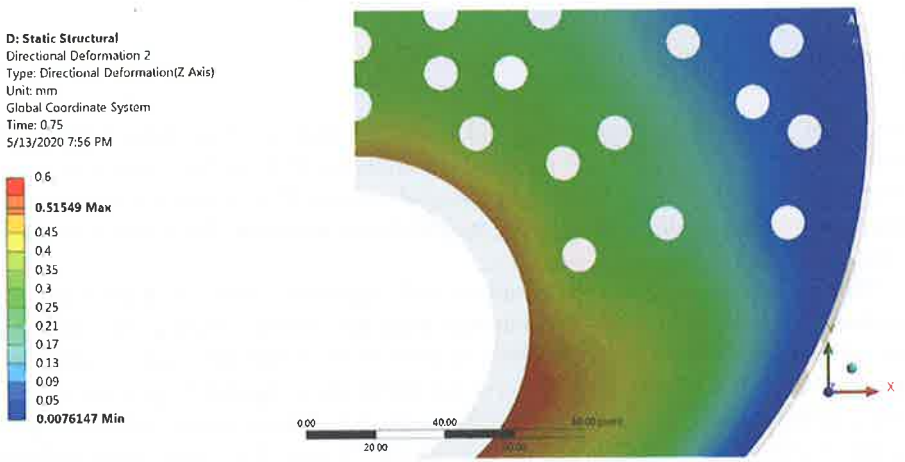

Fig. 12. Results of directional deformation done numerically by Ansys software package - pressure load 5 bar

the first reflecting chamber on the real boiler. The numerical analysis, which included several different stages with different loads and conditions, indicated the occurrence of pipe plate bending, especially in the part between the fire tube and the flue gas pipes.

The presented tests on the model aimed to confirm a numerical model in cold and warm states of the construction.

Table 3. Results of the directional deformations measured by DIC Aramis system and FEM analysis with surface heating

Pressure [bar]	Aramis system [mm]	FEM Ansys [mm]
1.5	$0.04 \div 0.12$	$1.7351 \cdot 10^{-3} \div 0.12087$
3.5	$0.15 \div 0.3$	$3.3521 \cdot 10^{-3} \div 0.24365$
5	$0.40 \div 0.50$	$7.6147 \cdot 10^{-3} \div 0.51549$

In all presented examination stages the values obtained by measured 3D DIC Aramis system has significant matches with values obtained using finite element method by Ansys software package. In this case, it can be said that numerical model has the quite similar behavior under the same loads as the model, both in cold and warm state of the analyzed construction. The verified numerical model can be used with great certainty in other similar tests that can be done on the model. The application of this method is especially important in pressure vessel units because it facilitates and simplifies operational tests, which are non-destructive and without any contacts, that can be applicable even in hard-to-reach places.

6 Conclusion

This paper presents the experimental and numerical analysis of modeled boiler tube plate. The novelty is analysis of full-field experimental DIC method used especially on critical boiler element in different operational regimes. Collected data improves the numerical model and allows to have full insight in constrains and deformations in such boiler elements.

The aim was to verify numerical model with measured values of strain. The geometrical model was designed to fulfill the real loads and materials used in the real boiler unit, as well as the laboratory conditions. Scaling of the model was done by using the numerical experiment in order to preserve the construction rigidity. Experimental procedure includes also one of the conventional methods for strain measurement (as strain gauge), as it is mentioned the application of 3D DIC System. The obtained results have the significant matches in both cases. This strain values are also compared to results conducted by finite element method using Ansys software package. Therefore the formed numerical model is completely verified and can be used for other model testing in order to improve the performances, reliability, safety of the unit and also the design of the boiler with similar geometry.

Acknowledgments. This research was financially supported by the Ministry of Education, Science and Technological Development of the Republic of Serbia.

This paper presents the results of the research conducted within the project "Research and development of new generation machine systems in the function of the technological development of Serbia" funded by the Faculty of Mechanical Engineering, University of Niš, Serbia.

References

1. Taler, J., Dzierwa, P., Taler, D., Harchut, P.: Optimization of the boiler start-up taking into account thermal stresses. Energy **92**(1), 160–170 (2015)
2. Alobaid, F., Karner, K., Belz, J., Epple, B., Kim, H.G.: Numerical and experimental study of a heat recovery steam generator during start-up procedure. Energy **64**, 1057–1070 (2014)
3. Kim, T.S., Lee, D.K., Ro, S.T.: Analysis of thermal stress evolution in the steam drum during start-up of a heat recovery steam generator. Appl. Therm. Eng. **20**(11), 977–992 (2000)
4. Krüger, K., Franke, R., Rode, M.: Optimization of boiler start-up using a nonlinear boiler model and hard constraints. Energy **29**(12–15), 2239–2251 (2004)
5. Dzierwa, P.: Optimum heating of pressure components of steam boilers with regard to thermal stresses. J. Therm. Stress. **39**(7), 874–886 (2016)
6. Dzierwa, P., Taler, D., Taler, J., Trojan, M.: Optimum heating of thick wall pressure components of steam boilers. In: Proceedings of the ASME 2014 Power Conference POWER2014, Baltimore, Maryland, USA, July 28–31 2014. American Society of Mechanical Engineers, Power Division (Publication) POWER (2014)
7. Gaćeša, B., Milošević-Mitić, V., Maneski, T., Kozak, D., Sertić, J.: Numerical and experimental strength analysis of fire-tube boiler construction. Tehnički vjesnik **18**(2), 237–242 (2011)
8. Gaćeša, B., Maneski, T., Milošević-Mitić, V., Nestorović, M., Petrović, A.: Influence of furnace tube shape on thermal strain of fire-tube boilers. Therm. Sci. **18**(Suppl. 1), S29–S47 (2014)
9. Živković, D., Milčić, D., Banić, M., Milosavljević, P.: Thermomechanical finite element analysis of hot water boiler structure. Therm. Sci. **16**(Suppl. 2), 443–456 (2012)
10. Čukić, R., Maneski, T.: Thermomechanical stress analysis of the hot-water boiler by FEM. In: Proceedings of the third International Congress of Thermal Stress 99, Cracow, Poland (1999)
11. Živković, D., Milčić, D., Banić, M., Mijajlović, M.: Numerical method application for thermomechanical analysis of hot water boilers construction. In: Proceedings of the 24th International Conference on Efficiency, Cost, Optimization, Simulation and Environmental Impact of Energy Systems – ECOS 2011, Novi Sad, Serbia, pp. 1351–1362 (2011)
12. Mancic, M., Zivkovic, D., Djordjevic, M., Rajić, M.: Optimization of a polygeneration system for energy demands of a livestock farm. Therm. Sci. **20**(Suppl. 5), S1285–S1300 (2011)
13. EN 12953 - Shell Boilers - General, Materials for pressure parts of boilers and accessories, Design and calculation for pressure parts, Requirements for equipment for the boiler
14. Rajic, M., Banic, M., Zivkovic, D., Tomic, M., Mančić, M.: Construction optimization of hot water fire-tube boiler using thermomechanical finite element analysis. Therm. Sci. **22**(Suppl. 5), 1511–1523 (2018)
15. Tanasic, I., Tihacek-Sojic, Lj., Mitrovic, N., Milic-Lemic, A., Vukadinovic, M., Markovic, A., Milosevic, M.: An attempt to create a standardized (reference) model for experimental investigations on implant's sample. Measurement **72**, 37–42 (2015)
16. Milosevic, M.: Polymerization mechanics of dental composites – advantages and disadvantages. Procedia Eng. **149**, 313–320 (2016). International Conference on Manufacturing Engineering and Materials, ICMEM 2016, 6–10 June 2016, Nový Smokovec, Slovakia, Publisher: Elsevier Ltd.

17. Jovicic, R., Sedmak, A., Colic, K., Milosevic, M., Mitrovic, N.: Evaluation of the local tensile properties of austenite-ferrite welded joint. Chem. Listy **105**, 754–757 (2011)
18. Mitrovic, N., Milosevic, M., Momcilovic, N., Petrovic, A., Miskovic, Z., Sedmak, A., Popovic, P.: Local strain and stress analysis of globe valve housing subjected to external axial loading. In: Key Engineering Materials, vol. 586, 214–217 (2014). Trans Tech Publications
19. Qian, C.F., Yu, H.J., Yao, L.: Finite element analysis and experimental investigation of tubesheet structure. J. Press. Vessel. Technol. **131**(1), 111–114 (2009)
20. Ju, Y.: The analysis of the stress and shift of tube plate and edge of manhole of boiler. J. Dalian Fish. Univ. **1**(1), 71–75 (2000)
21. Wu, G., Zhao, J.: The cause and prevention of the tube plate crack of one gas-fired boiler. Ind. Boil. **1**(1), 54 (2009)
22. Orteu, J.: 3-D computer vision in experimental mechanics. Opt. Lasers Eng. **47**, 282–291 (2009)
23. Pan, B., Wu, D., Yu, L.: Optimization of a three-dimensional digital image correlation system for deformation measurements in extreme environments. Appl. Opt. **51**, 440–449 (2012)
24. Sutton, M., Orteu, J., Hubert, W.: Image Correlation for Shape, Motion and Deformation Measurements: Basic Concepts, Theory and Applications. Springer, Berlin (2009)
25. Mitrovic, N., Petrovic, A., Milosevic, M., Momcilovic, N., Miskovic, Z., Tasko, M., Popovic, P.: Experimental and numerical study of globe valve housing. Chem. Ind. **71**(3), 251–257 (2017)
26. Milosevic, M., Milosevic, N., Sedmak, S., Tatic, U., Mitrovic, N., Hloch, S., Jovicic, R.: Digital image correlation in analysis of stiffness in local zones of welded joints. Tech. Gaz. **23**, 19–24 (2016)
27. Mitrovic, N., Petrovic, A., Milosevic, M.: Strain measurement of pressure equipment components using 3D DIC method. Struct. Integr. Procedia **13**, 1605–1608 (2018). 22nd European Conference on Fracture - ECF22
28. Milosevic, M., Mitrovic, N., Jovicic, R., Sedmak, A., Maneski, T., Petrovic, A., Aburuga, T.: Measurement of local tensile properties of welded joint using Digital Image Correlation method. Chem. Listy **106**, 485–488 (2012)
29. Lezaja, M., Veljovic, Dj., Manojlovic, D., Milosevic, M., Mitrovic, N., Janackovic, Dj., Miletic, V.: Bond strength of restorative materials to hydroxyapatite inserts and dimensional changes of insert-containing restorations during polymerization. Dent. Mater. **31**(2), 171–181 (2015)
30. Milosevic, M., Mitrovic, N., Sedmak, A.: Digital image correlation analysis of biomaterials. In: 15th IEEE International Conference on Intelligent Engineering Systems 2011, pp. 421–425 (2011)
31. Tanasic, I., Tihacek-Sojic, Lj., Milic-Lemic, A., Mitrovic, N., Milosevic, M.: Enhanced in-vivo bone formation by bone marrow differentiated mesenchymal stem cells grown in chitosan scaffold. J. Bioeng. Biomed. Sci. **1**(107), 2 (2011)
32. Mitrovic, A., Mitrovic, N., Maslarevic, A., Adzic, V., Popovic, D., Milosevic, M.: Thermal and mechanical characteristics of dual cure self-etching, self-adhesive resin based cement. Exp. Numer. Investig. Mater. Sci. Eng. **54**, 3–15 (2018)
33. Milosevic, M., Mitrovic, N., Miletic, V., Tatic, U., Ezdenci, A.: Analysis of composite shrinkage stresses on 3D premolar models with different cavity design using finite element method. Key Eng. Mater. **586**, 202–205 (2014)
34. Tanasic, I., Tihacek-Sojic, Lj., Milic-Lemic, A., Mitrovic, N., Mitrovic, R., Milosevic, M., Maneski, T.: Analysing displacement in the posterior mandible using digital image correlation method. J. Biochips Tissue Chips **S1**, 006 (2011)
35. ThyssenKrupp Materials International, Seamless Carbon Steel Pipe for High-Temperature Service. www.s-k-h.com

36. Lucefin Group, Tehnical Card – P235GH (2019). www.lucefin.com
37. Todorović, M., Živković, D., Mančić, M.: Breakdowns of hot water boilers, In: Proceedings of the 17th International Symposium on Thermal Science and Engineering of Serbia SIMTERM 2015, Soko banja, Serbia, 761–769 (2015)
38. Todorovic, M., Zivkovic, D., Mancic, M., Ilic, G.G.: Application of energy and exergy analysis to increase efficiency of a hot water gas fired boiler. Chem. Ind. Chem. Eng. Q. **20**(4), 511–521 (2014)
39. Rajic, M., Zivković, D., Banic, M., Mancic, M., Maneski, T., Milosevic, M., Mitrovic, N.: Experimental and numerical analysis of stresses in the tube plate of the reversing chamber on the model of the boiler. In: Proceedings of the 19th International Conference on Thermal Science and Engineering of Serbia, pp. 439–449 (2019)

Experimental Evaluation of Correlations of Evaporation Rates from Free Water Surfaces of Indoor Swimming Pools

Marko Mančić[1](✉), Dragoljub Živković[1], Mirjana Laković Paunović[1], Milena Mančić[2], and Milena Rajic[1]

[1] Faculty of Mechanical Engineering, University of Niš, Aleksandra Medvedeva 14, 18000 Niš, Serbia
marko.mancic@masfak.ni.ac.rs

[2] Faculty of Occupational Safety, University of Niš, Čarnojevića 10a, 18000 Niš, Serbia

Abstract. Indoor swimming pool buildings can be considered as significant energy consuming public buildings. Most energy is consumed to heat swimming pool water and maintain the desired thermal comfort conditions in the swimming pool hall. Water evaporation from the swimming pool water surface increases humidity in the pool hall air, and therefore the consumption of energy for heating and ventilation of the swimming pool and the hall increases, especially in the scenario of more strict humidity control of the pool hall air. Mathematical correlations for predicting the evaporation rates from free water surfaces can be found in literature, but not all of them were designed specifically for indoor swimming pools. In this paper, the properties of indoor swimming pool water, pool hall air and evaporation rates are measured in a real indoor swimming pool building and measurement results are presented in the paper. The measured results are confronted to the evaporation rates calculated by applying literature mathematical correlations for determination of evaporation rates. A large discrepancy of results from the literature is determined. Based on the original measured results, a mathematical correlation for estimation of evaporation rates of indoor swimming pools is created by application of the least square method.

Keywords: Evaporation · Measurement · Free water surface · Swimming pool

1 Introduction

Buildings with indoor swimming pool consume significant amount of energy for heating and ventilation. Energy in swimming pool building facilities is used for maintaining the thermal comfort conditions in the swimming pool hall, as well as for maintaining the pool water at desired temperature. In indoor swimming pool buildings 45% of energy is used for pool hall ventilation, and 33% for heating pool water. Heating and ventilation of the rest of the building accounts for around 10%, 9% of energy is used for lighting and equipment and sanitary hot water accounts for 3% of total energy consumption [1]. The highest thermal loads in indoor swimming pool buildings, often originates from water evaporation from the pool water surface [2].

N. Mitrovic et al. (Eds.): CNNTech 2020, LNNS 153, pp. 378–393, 2021.
https://doi.org/10.1007/978-3-030-58362-0_22

1.1 Water Evaporation in Indoor Swimming Pools

There are many mathematical models representing efforts to describe the physical phenomena of water evaporation from a free water surface [4–22] and most of them are empirical or semi-empirical, heavily relying on the results from experiments on either real objects or laboratory installations. Simultaneous transport of heat, mass and momentum occurring as well as the fact that this is phase flow process, make it's modelling difficult. In a general case, water evaporation rate from a surface depends on the air flow above the water surface, and the gradient of partial pressures of water vapor at water level and water vapor in the air above the surface of the water. Correlations for predicting water evaporation rate from a free water surface to both still and moving air can be found in literature [4–22]. Bowen provided a general solution for determination of heat transfer by convection and evaporation from a water surface of an element of volume for three different conditions [15]. In order to do this, he first determined a model of vapor diffusion from a unit area. Most of the correlations are based on the Dalton's theory, but there are also attempts of creating correlations based on analogy between heat and mass transfer [7, 15], where a ratio between conduction heat loss and evaporation heat loss is determined. Many evaporation models are analyzed or reviewed in literature [7–22], but even for detailed numerical simulations [16, 20] it is necessary to first determine the evaporation rate from the water surface and the evaporation rate coefficient.

Since the air velocity in indoor swimming pools originates from heating and ventilation equipment operation, it is usually kept at low levels. Heating and ventilation equipment of swimming pool halls usually consists of supply and return ducts spread on several locations through-out the hall, which cause complex air movement in the hall and contributes to forced evaporation. The correlations obtained by experiments for predicting evaporation rates from a water surface of indoor and outdoor swimming pools represent a function of air velocity above the water surface [7]. Air velocity over the indoor swimming pool water surface is not uniform, but extremely complex. The intensity and direction of the air velocity vector show large variations over time. This can be seen in results of a CFD simulation of a public swimming pool [20], where air temperature and humidity at the air return intake was measured and compared to the simulation results. Most of the simulated air velocities were up to 0.2 m/s, but there were also some slightly higher values. In addition, apart from air velocity, the nature of air flow over the water surface in indoor swimming pools has a strong influence on evaporation, which is determined by the value of Reynolds number and Sherwood numbers [15].

Evaporation Rate from Free Water Surface Correlations

The first equation of evaporation from free water surface was given by Dalton (1802) [6], when it was found to be proportional to the partial pressure difference of water vapor near the boundary surface p_a and away from the surface p_{sw}:

$$-dE = K(p_{sw} - p_a)df_{sw} \tag{1}$$

Where df_{sw} is an element of evaporation surface, E is evaporation rate per unit time, and K is a coefficient affected by properties of air flow over the boundary water surface.

According to Lewis the evaporation rate may be determined as:

$$-dE = K_E(x_{sw} - x)df_{sw} \tag{2}$$

Here, K_E is the evaporation rate coefficient given in (kg/s m^2), which is again affected by the properties of air flow over the boundary water surface and is usually given as a linear function of air velocity:

$$K = A + BV_a \tag{3}$$

Where, V_a is the velocity of air above the free water surface, A and B are correlation constants. Values of this coefficient from literature are given in Table 1.

Table 1. Literature evaporation rate prediction correlations

Author	Correlation coefficients of Eq. (3)	Application
McMilan	A = 0.0360; B = 0.250	Lakes
Chernecky	A = 0.05053; B = 0.06638	Swimming pools
Carrier	A = 0.088403; B = 0.001296	Solar pond
Hahne and Kübler	A = 0.0850 B = 0.0508	Outdoor swimming pools
Rohwer	A = 0.0803; B = 0.0583	Laboratory model
Smith et al.	A = 0.0888; B = 0.0583	Swimming pool
Smith et al.	A = 0.0638; B = 0.0669	Outdoor swimming pool
Himus and Hinchey	A = 0.1538; B = 0.06898	General
Lurie and Michailoff	A = 0.109; B = 0.0859	General

A review and comparison of mathematical models for predicting evaporation rates by Sartori [7], indicated a large scattering of results obtained using investigated literature correlation models. Some of the models neglect the influence of relative humidity of the air. Sartori provided a correlation model, where evaporation is a coefficient of air velocity to the power of 0.8, and length of the water surface, instead of actual water surface. Shah proposed a model where evaporation rate coefficient equals to 0.00005 [21, 22]. Asdrubali et al., determined values of the correlation coefficients for air velocity values of 0.05 m/s, 0.08 m/s and 0.17 m/s, equal to 3.4×10^{-8}, 4.2×10^{-8} and 5.2×10^{-8} respectfully, based on results from a laboratory indoor swimming pool scale model [5].

A comparison of the evaporation rates obtained using the correlations in Table 1, are given in Fig. 1. It is clear, that a significant discrepancy of the results can be found.

2 Determination of Evaporation Rates and Water and Air Properties by Real Object Measurement

Having in mind that empirical equations strongly depend on the experimental conditions, as well as the results they are based on. According to Sartori, one empirical evaporation prediction equation is necessary for each class of these conditions [7]. There are

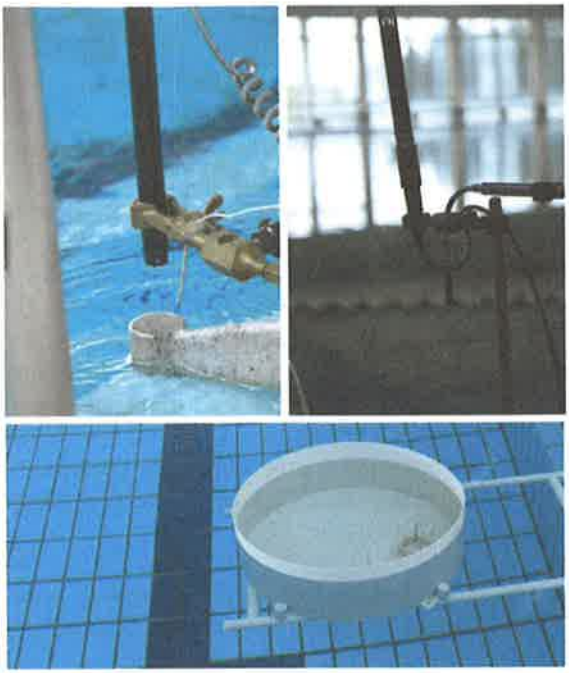

Fig. 1. Apparatus used for measuring on a real swimming pool

differences of height of the point above water level where air velocity is measured, which usually ranges from 0.3–10 m, however most of the heights range from 0.5–2 m for which the differences in results are not significant and are considered not to affect results [3, 5, 7, 10–14]. Smith et al. performed measurements on an outdoor swimming pool, where water body temperature was kept at 28.9 °C, which was monitored using thermocouples. Pool water level was monitored using a Microtector gauge, whereas wind speed was monitored using a rotating cup anemometer at 0.3 m above the pool. Tang and Etzon, compared water evaporation from free water surface and wetted water surface, for which they constructed two identical water "ponds", and found that the evaporation rate of from a free water surface is proportional to the difference in partial pressure of water vapour at water temperature and air above it to the power of 0.82 [4]. Ruiz and Martinez measured relevant parameters of water and air at the border of an out-door pool, at 0.5 m above water level, and water temperature was measured 1 m below water surface, but evaporation rate was not measured, instead it was calculated using correlations from the literature which lead to difference in results [8]. Asdrubali created a scale model of an indoor swimming pool, and measured evaporation rates for air velocities of 0.05 m/s, 0.08 m/s, 0.17 m/s and relative humidity 0.5, 0.6 and 0.7 [2], but the air flow in the laboratory model could be considered uniform and the air flow originating from a typical duct ventilation system in a pool hall is extremely complex. Smith et al. [10] used shallow aluminum floating evaporation pans with diameter of 20 cm, to determine short term evaporation from an out-door swimming pool, but such

small pan evaporation surface and the air flow above it are either affected by pan walls, or permit water penetration, thus affecting reliability of the results.

Results presented in this paper were acquired by measuring air flow velocities at 5 points along the pool border, at 0.65 m above water level in the direction of the air flow coming from the ventilation ducts. Average air velocities ranged from 0.01 m/s to 0.07 m/s at the opposite ends of the pool border, and from 0.15 m/s to 0.34 m/s at the middle of the pool border. Water temperature was measured 1 cm below water level using a thermo K type couple probe. Relative humidity and temperatures were measured 1 cm above the water level and 90 cm above water level. Evaporation rate was measured hourly using an evaporation pan with a needle, with a diameter of 0.8 m immersed in the pool water 1.3 m from the pool border. The diameter of the evaporation pan was chosen so it would be big enough to account for the affect of the complex air flow above the water surface in the pool hall. Evaporated water is measured with precision of 1 g, hourly.

Results are measured and collected in a the hall of active indoor swimming pools, in the Sport and Recreation Center Dubočica, Leskovac, in the period from May to August. The following apparatuses were used (Fig. 1):

1. TESTO 454 with 0420 relative humidity and air temperature probe,
2. Cole Palmer 37950-12 relative humidity sensor with air temperature probe,
3. AIRFLOW TA5 anemometer with thermometer,
4. K type thermocouple probe,
5. Evaporation pan with a needle.

Some of the evaporation rate results are discarded, since they were affected by activity of the swimmers causing water penetration into the evaporation pan. Evaporation rate E as function of air velocity Va is given in Fig. 1.

In Fig. 2, measured evaporation rates are presented as a function of the difference of partial pressures of saturated water vapour at water surface temperature and partial pressure of water vapour of air above water level (Eq. 4), calculated in Pa according to IAPWS Industrial Formulation for the Thermodynamic Properties of Water and Steam.

It can be observed from Fig. 2 and Fig. 3 that the evaporation rates mostly rise with the increase of air flow velocity above the water surface, and generally rise with the increase of difference of water pressures of water saturated water vapour at water surface and water vapour in the air above the water surface.

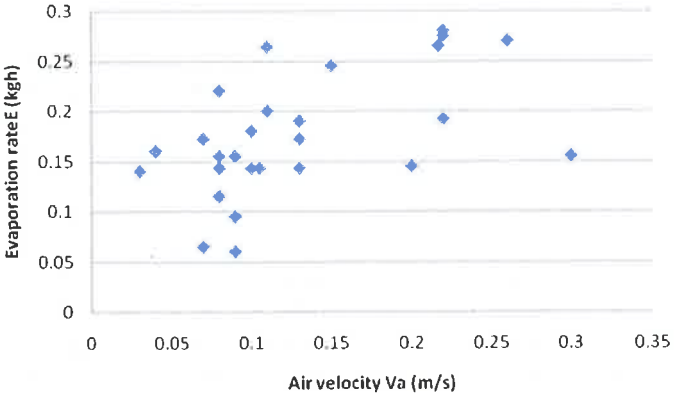

Fig. 2. Measured evaporation rates as a function of measured air velocity

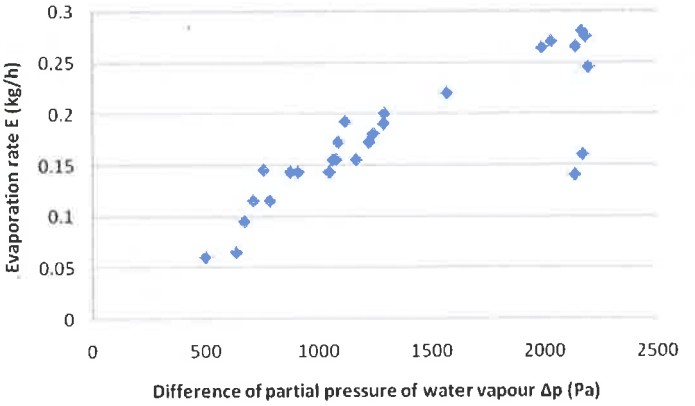

Fig. 3. Measured evaporation rates as a function of difference of partial pressures of water vapour

This is kind of relationship is in accordance with the majority of correlations found in literature. The measured results also showed a strong dependence on the air flow velocity. A significant drop of air velocity caused by the swathed off ventilation system, caused a drop of air velocity to near zero values (Fig. 2), which led to low values of evaporation rates despite relatively high partial pressure difference gradient. This can be observed in Fig. 3.

3 Comparison of Measured Results and Literature Correlation Calculated Results

Obtained measurement results are compared to the values of evaporation rates, obtained for the same air and water parameter values by calculations using correlations from the literature (Table 1). Most of the evaluated results from literature correspond to outdoor swimming pools [3, 5, 8, 10] representing usually higher air flow velocities which

originate from wind, and are affected by direct solar radiation. Asdrubali [5] measured evaporation for air velocities of 0.05 m/s, 0.08 m/s and 0.17 m/s, which is a good match to air velocities found in a real indoor swimming pool hall, and reported evaporation rates in the range from 0.07–0.15 kg/h for relative humidifies between 50% and 70%. His results show a decrease of evaporation rates with increase of relative humidity of ambient air, which is related to the trend of change of the difference of partial pressures of water vapour at water temperature and air above the water level. One evaporation coefficient was determined for each of the tested cases, however a correlation as a general solution of the problem in the tested domain was not reported.

In his research, the temperature difference of water and air was kept constant at 2 °C. Although this is a recommended temperature difference value found in engineering design handbooks [4], other scenarios actually occur more often in reality. Shah [21, 22] provided correlations for predicting evaporation rates of indoor swimming pools, but he used data from literature to fit correlation curves, which is again limited by the covered domain and combination of conditions. Hence, in this paper measured data are compared to the values obtained by using correlations for calculating evaporation rates found in literature with correlation coefficients defined in Table 1. An illustration of the results obtained using most typically used correlations from literature, compared with the measured data are presented in Fig. 4.

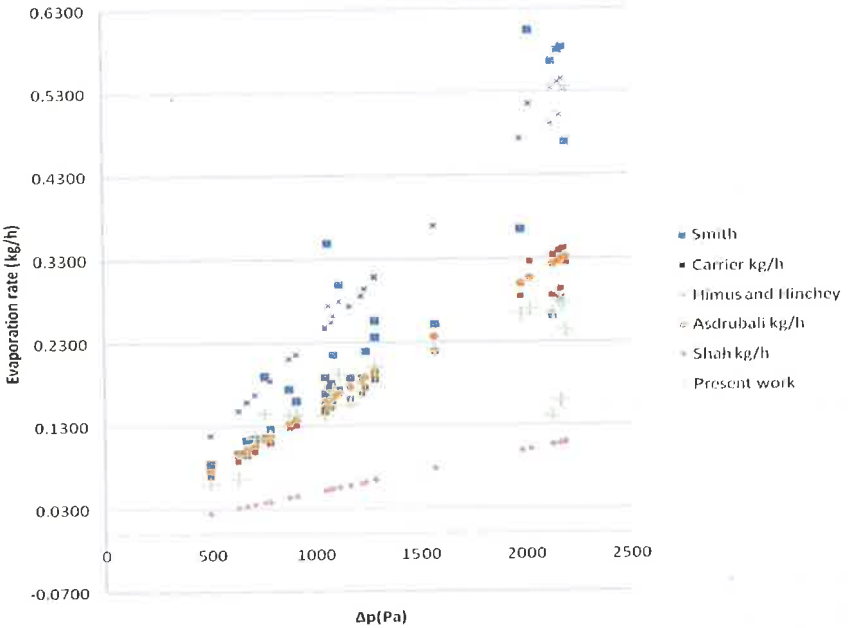

Fig. 4. Measured evaporation rates as a function of difference of partial pressures of water vapour compared to literature correlation results

It can be observed that some of the correlations, such as Smith's and Himus and Hinchey's significantly overestimate the evaporation rate for indoor swimming pools,

while Shah's correlation underestimates the Evaporation rate of indoor swimming pools. It is clear, that literature equations can lead to significant errors in prediction of evaporation rates from indoor swimming pools, and as such should be used with caution.

Based on the measured results, a mathematical correlation of the water evaporation rate from an indoor swimming pool is fitted by application of the method of least squares. A general mathematical form for correlations of water evaporation rate from free water surface, based on literature, was used, where values of mathematical symbols A, B and N were determined by application of the least squares method. The general mathematical representation of the evaporation rates from the free water surface, with thorough analysis of the literature correlations, suitable for numerical simulations of the behavior of indoor swimming pools can be written as [21] (Fig. 5):

$$\dot{E} = \left(AV_a^N + B\right)\left(\mathrm{p_{sw}} - \varphi \mathrm{p_a}\right)/\mathrm{r} \tag{4}$$

Here, the evaporation rate is obtained as time dependent value, in kg/s. Factors A, B and N in the Eq. (4), should be determined based on empirical, i.e. measured results, where r is the latent heat of water evaporation. Based on the fitting of correlation curve with respect to measured results, the following correlation factors are determined to provide the best fit, i.e. least correlation error value, as written in Eq. (5) for the evaporation coefficient K with respect to Eq. (3):

$$K = 1.636585(0.000085643V_a + 0.66206089)^{1.1945}. \tag{5}$$

The results of the obtained evaporation rates in kg/h using the correlation in Eq. (5), are presented in Fig. 6 and 7. The Fig. 6 shows estimated evaporation rate for the temperature of air above the pool of 22 °C, with respect to relative humidity of Rh = 50% and Rh = 60%, and water temperature in the range from 26 °C to 29 °C. Figure 7 presents change of the estimated evaporation rate using Eq. (4), with respect to the change of partial differential pressure difference between the saturated air and air above the water surface.

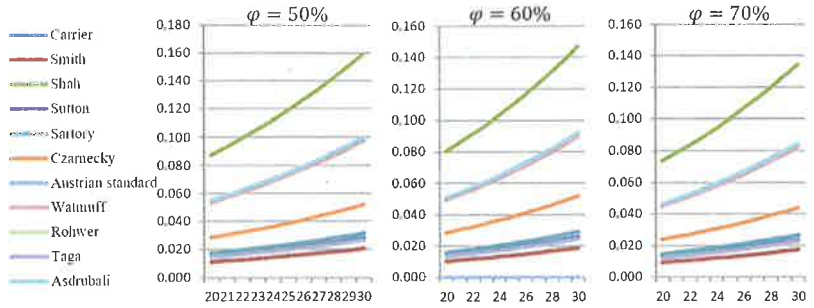

a) Evaporation rates obtained using evaporation coefficients from table 1. in kg/m²h for air velocity of 0.05m/s, and relative humidity of 50%, 60% and 70%, respectfully.

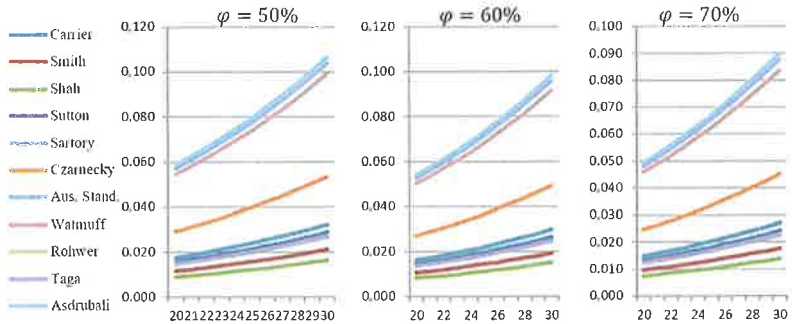

b) Evaporation rates obtained using evaporation coefficients from table 1. in kg/m²h for air velocity of 0.08m/s and relative humidity of 50%, 60% and 70%, respectfully.

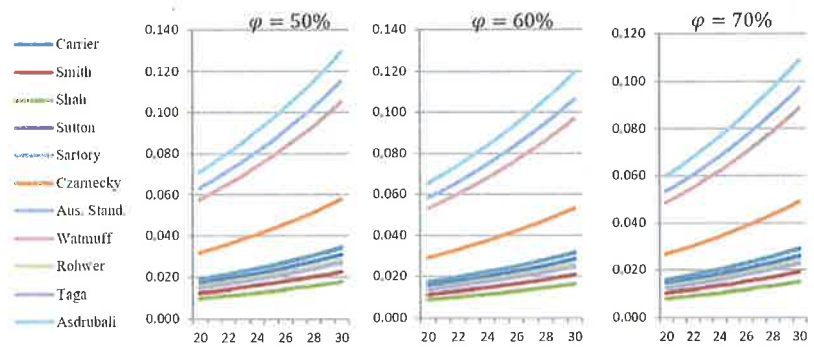

c) Evaporation rates obtained using evaporation coefficients from table 1. in kg/m²h for air velocity of 0.17m/s and relative humidity of 50%, 60% and 70%, respectfully.

Fig. 5. Comparison of the evaporation rate results obtained for the correlation coefficients obtained with evaporation rate swimming pool correlations

The results obtained by applying the proposed mathematical correlation are compared to the actual measured results, for the values of the variables in the Eq. (4) obtained by measurements in the real object. The results obtained using the proposed correlation in Eq. (4), using the evaporation coefficient from Eq. (5). Show very good agreement

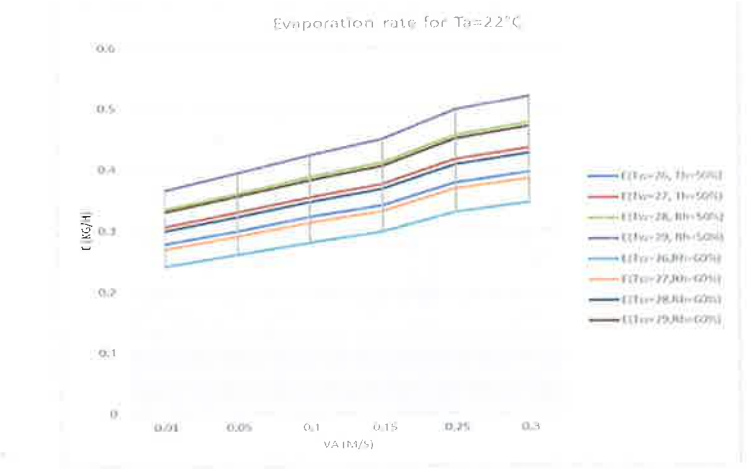

Fig. 6. Estimated pool water evaporation rates using the mathematical correlation obtained based on the measured results, with respect to relative humidity and pool water temperature, for indoor pool hall temperature of 22 °C

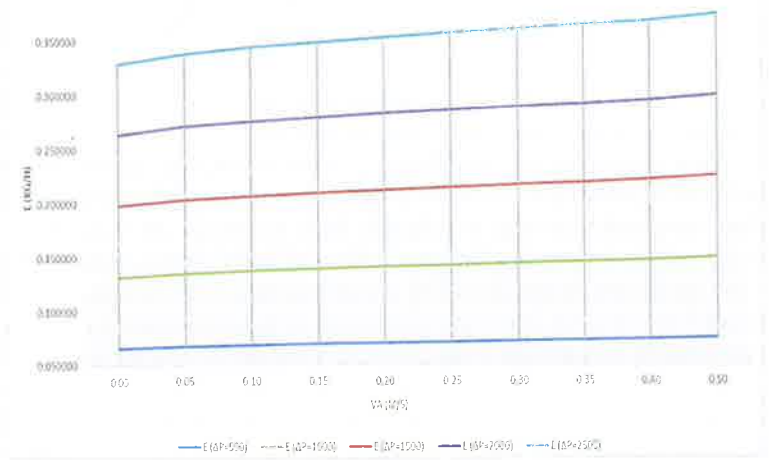

Fig. 7. Estimated evaporation rates in kg/h with respect to the change of partial differential pressure difference in Pa between the saturated air and air above the water surface.

with the measured results (Fig. 8). There is a significant disagreement with the measured results in one point, for the air velocity Va = 0.07 m/s. The significant difference could have occurred partially due to the normal imperfection of the mathematical approximation, and partially due to measurement error at the point of disagreement.

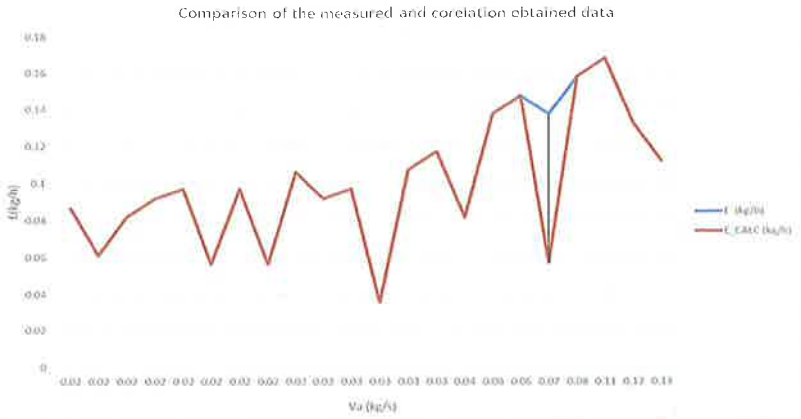

Fig. 8. The results obtained by applying the proposed mathematical correlation compared to the actual measured results

4 Energy Balance of the Indoor Swimming Pool with Application of the Obtained Evaporation Rate Correlation Equation

The obtained mathematical correlation was formed to be suitable for numerical quasistatic simulations of the energy performance of the swimming pool, as presented in [21, 22]. The obtained correlation was applied in a Trnsys swimming pool model, as part of the energy balance of the indoor swimming pool.

In the indoor swimming pool buildings, systems for heating, air conditioning and ventilation are designed to provide suitable thermal comfort conditions in the pool hall areas. Indoor temperature is kept at relatively high levels (24–30 °C), which creates conditions for significant evaporation rates from pool water surface. Relative humidity, as one of the significant factor should be maintained below recommended values not only for comfort reasons, but also to prevent corrosion and condensation problems in the pool facility areas. It is important to identify and maintain an optimal ratio between air temperatures, pool water temperature and air velocity in the pool hall, in order to achieve lower energy consumption for heating in the building. The modelling approach for indoor swimming pools presented in [21, 22] is applied to model the indoor swimming pool building analyzed in the paper. The pool water temperature change is calculated as [21, 22]:

$$\rho_w c_{pw} V_p \frac{dT}{d\tau} = \underset{aux}{\dot{Q}} - \left(\underset{fw}{\dot{Q}} + Q_{evap} + Q_{conv} + Q_{rad} \right)$$

$$= \underset{aux}{\dot{Q}} - \underset{fw}{\dot{Q}} - A_p \left(\dot{E}\, r + \alpha (T_w - T_{air}) + \varepsilon \sigma \left(T_w^4 - T_{wall}^4 \right) \right) \qquad (6)$$

Where: Evaporation heat losses Q_{evap} are a function of mass flow rate of evaporated water $\dot{E}$ and the latent heat of evaporation r; heat transfer by convection from the water surface Q_{conv} is a function of the convective heat transfer coefficient α, temperature of

the pool water T_w and the indoor air temperature in the pool hall T_{air}; radiation losses Q_{rad} is the function of the emissivity ε[-], the Stefan-Boltzmann constant $\sigma = 5.67 \cdot 10^{-18}[Wm^{-2}K^{-4}]$ and temperature of the indoor wall surface T_{wall}; Q_{fw} is the heat loss caused by supply of fresh water; and Q_{aux} is the heat gain from auxiliary heating equipment. The total water surface of the pool water area A_p is 1480 m^2. A balance model of an indoor swimming pool is presented in [22].

Evaporation heat losses are proportional to the flow of evaporated water from the water surface of the swimming pool:

$$q_E = \dot{E} \cdot r \tag{7}$$

Where $\dot{E}$ is the mass flow rate of evaporated water and r is the latent heat of evaporation. Heat transfer from convection from the water surface per unit surface area can be presented as:

$$q_{con} = \alpha(t_w - t_a) \tag{8}$$

Where α is the heat transfer coefficient, T_w is temperature of the pool water and T_a is the indoor air temperature in the pool hall. Convective heat transfer coefficient can be expressed as [22]:

$$\alpha = 2.8 + 3.0 \cdot V_a \tag{9}$$

Where V_a stands for air velocity above the water surface.

Radiation losses are calculated according to Stefan-Boltzmann law to sky for outdoor swimming pools are considered in [22]. The proposed model of the indoor swimming pool includes the heat transfer by radiation exchange with pool hall walls per unit of pool area [22]:

$$q_{rad} = \varepsilon \cdot \sigma \cdot \left(T_w^4 - T_{wall}^4\right) \tag{10}$$

Where ε is the emissivity average and σ is the Stefan-Boltzmann constant ($\sigma = 5.67 \cdot 10^{-8} \frac{W}{m^2 \cdot K^4}$) and T_{wall} is the temperature of the wall surface.

For the proposed swimming pool water it is assumed to have a constant water level in the pool. The mass of the evaporated water and waste water losses in the water treatment plant are compensated by fresh water supply system. Heat loss caused by supply of fresh water with lower temperature than that of the pool can be calculated by [22]:

$$\dot{Q}_{fw} = \dot{m_{fw}} \cdot c_{pw} \cdot \left(t_w - t_{fw}\right) \tag{11}$$

The heat losses should be compensated by heat gains in the pool area. Heat gains from auxiliary heating equipment to the swimming pool can be expressed as [22]:

$$\dot{Q}_{aux} = \dot{m_{aux}} \cdot c_{pw} \cdot (t_w - t_{aux}) \tag{12}$$

Where $\dot{m}_{aux}$ is the mass flow rate supplied by the auxiliary heating equipment, and t_{aux} is the temperature water supplied for auxiliary heating.

Hence, energy balance of the swimming pool can be written as [22]:

$$\dot{Q}_{aux} - \dot{Q}_{fw} - A_p \cdot (q_E + q_{con} + q_{rad}) = 0 \tag{13}$$

The simulation results in [22] indicate that the impact of radiation to the energy balance of the pool is negligible small.

The indoor swimming pool building facility was modeled as a multizone building in Trnsys software, with the envelope properties of the building described in [21, 22], thus determining the annual behavior of heating and cooling loads. The building was modelled as multi-zone in TRNSYS software [22]. Air velocity of 0.08 m/h in the swimming pool hall was assumed constant, determined based on the measured data. The simulation was done using the Meteonorm hourly weather data, which also included mains water temperature used for fresh water supply system.

The simulated results for the same ambient temperatures were compared with the measured results (Fig. 9, 10 and 11). The comparison of the results showed acceptable difference of results. The presented values of the simulated data in Fig. 9, 10 and 11 are rounded to values with two decimal places for easier comparison. Although a good agreement of the results of the simulation and the measured results on the real object is found, as presented in Fig. 9, 10 and 11, there is still slight error in the simulation results. This can be attributed to the complex mathematical model applied in Trnsys software, where, for the purpose of the simulation whose results re-presented in this paper, the heating and ventilation equipment was also modeled and all of this affects simulation result.

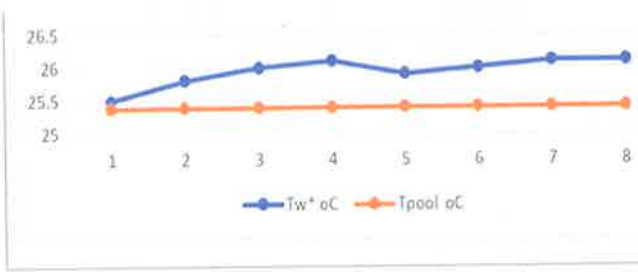

Tw [°C]	Tpool [°C]
25.5	25.38
25.8	25.39
26.0	25.39
26.1	25.39
25.9	25.40
26.0	25.40
26.1	25.40
26.1	25.41

Fig. 9. Measured pool water temperature (T_{pool}) and simulated pool water temperature (T_w)

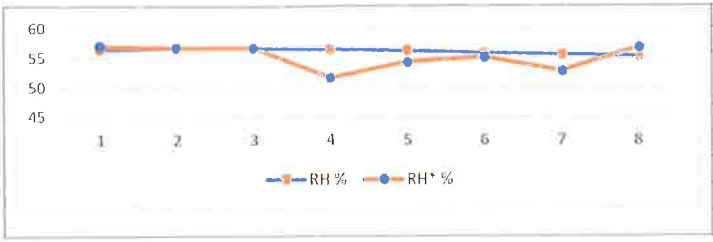

RH* [%]	RH[%]
57,0	56,55
56,7	56,70
56,7	56,74
51,7	56,51
54,4	56,19
55,1	55,82
52,8	55,57
56,8	55,31

Fig. 10. Measured relative humidity of the pool hall air (RH*) and the simulated relative humidity of the pool hall air RH

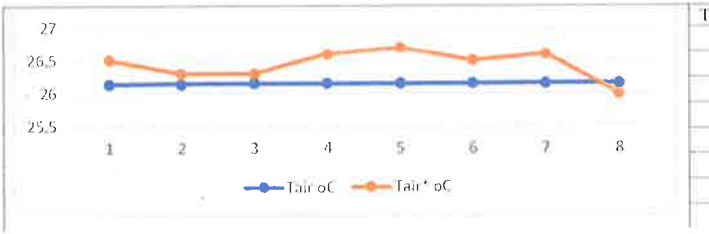

Tair [°C]	Tair* [°C]
26,14	26,5
26,14	26,3
26,14	26,3
26,14	26,6
26,14	26,7
26,15	26,5
26,15	26,6
26,15	26,0

Fig. 11. Simulated air temperature in the pool hall (T_{air}) compared to the measured temperature of pool hall air (T_{air}*)

5 Conclusion

This paper presents literature correlations for evaluation of the evaporation rates from free water surfaces, and applies them for estimation of this phenomenon in indoor swimming pools. Water evaporation from the water surface of an indoor swimming pool was also measured, as well as relevant parameters for its prediction. Measured results are presented in the paper and compared to the results calculated using available literature mathematical correlations for predicting evaporation rates from a water surface from the literature. It was found that most of the equations either overestimate or underestimate the evaporation rates, which implies extreme caution for their application for analysis of indoor swimming pools.

A new correlation should be fitted according to the measured data to ensure good prediction of evaporation rates for the purpose of predicting evaporation rates of indoor swimming pools. The measured data represents actual data found in a real indoor swimming pool building, while the measured air and water properties represent actual values found in operation of a real object. The domain covered by the measured parameters should be sufficient for creating a new correlation valid for typical conditions found in real indoor swimming pool buildings.

Acknowledgement. This research was financially supported by the Ministry of Education, Science and Technological Development of the Republic of Serbia.

References

1. Trianti-Stourna, E., Spyropoulou, K., Theofylaktos, C., Droutsa, K., Balaras, C.A., Santamouris, M., Asimakopoulos, D.N., Lazaropoulou, G., Papanikolaou, N.: Energy conservation strategies for sports centers: Part B. Swimming pools. Energy Build. **27**, 123–135 (1998)
2. Asdrubali, F.: A scale model to evaluate evaporation from indoor swimming pools. Energy Build. **41**, 311–319 (2009)
3. Hahne, E., Kübler, R.: Monitoring and simulation of the thermal performance of solar heated outdoor swimming pools. Sol. Energy **53**(1), 9–19 (1994)
4. ASHRAE HVAC Application Handbook, Atlanta, GA (1999)
5. Auer, T.: Assessment of an indoor or outdoor swimming pool, TRNSYS-TYPE 144, Transsolar, Energietechnik GMBH (1996)
6. Dalton, J.: Experimental essays on the constitution of mixed gases; on the force of steam or vapor from water and other liquids in different temperatures, both in a Torricellian vacuum and in air; on evaporation on the expansion of gasses by heat. Mem. Manchester Liter. Phil. Soc. **5–11**, 535–606 (1802)
7. Sartori, E.: A critical review on equations employed for the calculation of the evaporation rate from free water surfaces. Sol. Energy **68**(1), 77–89 (2000)
8. Ruiz, E., Martinez, P.J.: Analysis of an open-air swimming pool solar heating system by using an experimentally validated TRNSYS model. Sol. Energy **84**, 116–123 (2010)
9. Tang, R., Etzion, Y.: Comparative studies on the water evaporation rate from a wetted surface and that from a free water surface. Build. Environ. **39**, 77–86 (2004)
10. Smith, C.C., Lof, G., Jones, R.: Measurement and analysis of evaporation from an inactive outdoor swimming pool. Sol. Energy **53**(1), 3–7 (1994)
11. Mitrovic, N., Petrovic, A., Milosevic, M., Momcilovic, N., Miskovic, Z., Tasko, M., Popovic, P.: Experimental and numerical study of globe valve housing. Chem. Ind. **71**(3), 251–257 (2017)
12. Rajic, M., Banic, M., Zivkovic, D., Tomic, M., Mančić, M.: Construction optimization of hot water fire-tube boiler using thermomechanical finite element analysis. Therm. Sci. **22**(Suppl. 5), 1511–1523 (2018)
13. Milosevic, M., Mitrovic, N., Jovicic, R., Sedmak, A., Maneski, T., Petrovic, A., Aburuga, T.: Measurement of local tensile properties of welded joint using Digital Image Correlation method. Chem. Listy **106**, 485–488 (2012)
14. Todorovic, M., Zivkovic, D., Mancic, M., Ilic, G.: Application of energy and exergy analysis to increase efficiency of a hot water gas fired boiler. Chem. Ind. Chem. Eng. Q. **20**(4), 511–521 (2014)
15. Bowen, I.S.: The ratio of heat losses by conduction and by evaporation from any water surface. Phys. Rev. **27**, 779–787 (1926)
16. Heiselberg, L.Y.: CFD Simulations for Water Evaporation and Airflow Movement in Swimming Baths, Report for the project "Optimization of Ventilation System in Swimming Bath". Aalborg University, Denmark (2005)
17. Shah, M.: Prediction of evaporation from occupied indoor swimming pools. Energy Build. **35**, 707–713 (2003)
18. Shah, M.: Improved method for calculating evaporation from indoor water pools. Energy Build. **49**, 306–309 (2012)
19. Moghiman, M., Jodat, A.: Effect of air velocity on water evaporation rate in indoor swimming pools. Iran. J. Mech. Eng. **8**, 19–30 (2007)
20. Vinnichenko, N.A., Uvarov, A.V., Vetukov, D.A., Plaksina, Y.Y., Direct computation of evaporation rate at the surface of swimming pool, in Recent research in mechanics. In: Proceedings of the 2nd International Conference on Fluid Mechanics and Heat and Mass Transfer, Corfu island, Greece (2011)

21. Mančić, M.V., Živković, D., Đorđević, M.Lj., Jovanović, M.S., Rajić, M.N., Mitrović, D.M.: Techno-ecnomic optimization of configuration and capacity of a polygeneration system for the energy demands of a public swimming pool building. Therm. Sci. **22**(5), 1535–1549 (2018)
22. Mančić, M.V., Živković, D., Đorđević, M.Lj., Jovanović, M.S., Rajić, M.N., Mitrović, D.M.: Mathematical modelling and simulation of the thermal performance of a solar heated indoor swimming pool. Therm. Sci. **18**(3), 999–1010 (2014)